Res Intell Manuf Assem, 2026, 5(1): 361-381
DOI: 10.25082/RIMA.2026.01.005

RESEARCH ARTICLE

Smart Polymeric Liners for Internal Corrosion Control in Wet Sour Gas Pipelines: Integrating Nanostructured Materials and AI-Driven Predictive Modelling

Mavis Sika Okyere

Department of Pipelines and Stations, Ghana National Gas Limited Company, Accra, Ghana

Correspondence to: Mavis Sika Okyere, Department of Pipelines and Stations, Ghana National Gas Limited Company, Accra, Ghana;
Email: mavis.nyarjko@ghanagas.com.gh

Received: January 7, 2026;
Accepted: April 26, 2026;
Published: April 29, 2026.

Citation: Okyere MS. Smart Polymeric Liners for Internal Corrosion Control in Wet Sour Gas Pipelines: Integrating Nanostructured Materials and AI-Driven Predictive Modelling. *Res Intell Manuf Assem*, 2026, **5**(1): 361-381.
https://doi.org/10.25082/RIMA.2026.01.005

Abstract: Sour gas pipelines suffer severe integrity challenges due to internal corrosion driven by hydrogen sulfide (H_2S) and carbon dioxide (CO_2). This study introduces a novel smart polymeric liner enhanced with nanostructured graphene and Nano silica fillers, integrated into a CFD→AI→digital twin workflow for predictive corrosion control. Unlike conventional inhibitors and coatings, the liner combines Nano-structural impermeability, mechanical reinforcement, and tailored interfacial adhesion strategies to suppress corrosion in API 5L X65 steel pipelines. CFD simulations under synthetic worst case conditions produced an upper bound corrosion rate of 2703.66 mm/year for bare steel. This value is explicitly presented as a theoretical limit to illustrate the severity of unprotected sour service. Under typical industrial operating conditions, predicted rates fall within the 1–5 mm/year range, consistent with field data. Service life predictions are conservatively adjusted to account for liner aging, mechanical wear, and interfacial debonding, yielding a practical range of 20–30 years. An AI regression model trained on CFD outputs and experimental data achieved $R^2 \approx 0.99$, enabling accurate forecasts of corrosion rates and remaining life. Integration into a digital twin framework allows real-time monitoring, predictive maintenance scheduling, and dynamic risk assessment. This work establishes a next-generation material–digital solution for extending the service life of sour gas pipelines.

Keywords: smart materials, polymeric liners, sour gas corrosion, Hydrogen Sulfide (H_2S), Computational Fluid Dynamics (CFD), Artificial Intelligence (AI), machine learning

1 Introduction

Sour gas pipelines, which are essential for global energy transport, face severe risks of internal corrosion and hydrogeninduced degradation due to the presence of hydrogen sulfide (H_2S) and carbon dioxide (CO_2) [1, 2]. Conventional mitigation methods, such as chemical inhibitors, cathodic protection, and metallic coatings, often lack durability and consistency under aggressive sour gas conditions [3, 4], underscoring the need for advanced solutions.

Smart polymeric liners enhanced with nanostructured materials offer a promising approach by providing impermeability, chemical resistance, and strong adhesion to steel substrates [5, 6]. Recent advances in nanocomposites, incorporating fillers such as silica, graphene, and titanium dioxide, have improved barrier properties and mechanical strength, addressing limitations of earlier polymer coatings [7, 8].

Complementing material innovation, computational fluid dynamics (CFD) and artificial intelligence (AI) provide powerful tools for predictive integrity management [9, 10]. CFD enables mechanistic modelling of fluid flow, species transport, and localized corrosion, while AI learns from experimental and simulation data to forecast corrosion rates and pipeline remaining life [11]. Integrated within digital twin frameworks, these approaches enable real-time monitoring, predictive maintenance, and optimized asset management [12]. Recent investigations highlight the superior corrosion resistance of polymer nanocomposites reinforced with graphene and silica fillers.

Polymer/Graphene Systems: Avantgarde polymer/graphene nanocomposites demonstrate enhanced impermeability, mechanical robustness, and electrochemical stability under aggressive sour gas conditions. Studies report significant reductions in corrosion current density and improved adhesion compared to conventional epoxy coatings [13, 14]. A 2025 review empha-

sised graphene's multifunctionality—high surface area, conductivity, and inertness, making it a versatile filler for both energy storage and corrosion protection applications [15].

Polymer/NanoSilica Systems: Silica/polymer nanocomposites leverage tunable morphology and high surface area to improve barrier performance. Experimental work shows reduced water and gas permeability, improved mechanical strength, and better dispersion of silica nanoparticles within epoxy matrices [16]. A 2024 review of Nanobased smart coatings confirmed silica's role in enhancing corrosion inhibition while reducing reliance on toxic inhibitors [17].

The performance of nanocomposite liners is governed by several synergistic mechanisms:

(1) Tortuosity and Reduced Permeability: Impermeable fillers (graphene sheets, silica particles) force corrosive species to follow longer, more tortuous diffusion paths, thereby reducing permeation rates [18].

(2) Mechanical Reinforcement: Nanofillers improve tensile strength, modulus, and fracture toughness, mitigating liner damage under sour gas pressure and temperature fluctuations [19].

(3) Interfacial Adhesion Strategies: Surface functionalization of graphene and silica (e.g., silane coupling agents, oxygenated groups) enhances chemical bonding with polymer matrices, reducing delamination and improving longterm durability [20].

Industrial deployment of polymer liners in sour gas pipelines has been explored, but challenges remain:

(1) Non-Metallic Pipe (NMP) Liners: Widely used as internal linings, these systems face permeation damage, creep, fatigue, and installation defects, limiting their reliability in high-pressure sour environments [21].

(2) SourResistant Line Pipe Steels: While steels with SSC resistance are available, failures under severe H_2S conditions highlight the need for hybrid solutions combining metallic substrates with advanced polymeric liners [22].

(3) Case Studies: Lifecycle analyses of sour wet gas pipelines (2018–2024) reveal fluctuating corrosion risks, underscoring the importance of adaptive liner systems integrated with predictive monitoring [23].

Coupling advanced liners with CFD and AIdriven models enhances predictive reliability:

(1) CFD simulations capture localised flow regimes and species transport in sour gas pipelines, identifying high-risk zones for liner degradation [24].

(2) AI models trained on experimental and simulation datasets forecast corrosion rates and liner performance, enabling real-time monitoring within digital twin frameworks [25].

Despite decades of research into sour gas pipeline integrity, three critical gaps remain:

(1) Materials Gap: Conventional polymer liners and metallic coatings suffer from permeability, poor adhesion, and mechanical instability under high H_2S/CO_2 conditions. While nanostructured composites show promise, their performance in realistic operating environments has not been systematically validated.

(2) Mechanistic Modelling Gap: CFD has been applied to study fluid flow and corrosion interactions, but it is often computationally intensive, casespecific, and not scalable for predictive integrity management across diverse pipeline systems.

(3) Predictive Analytics Gap: AI models have been explored in corrosion research, but they are rarely integrated with mechanistic CFD outputs and realtime sensor data, limiting their ability to forecast corrosion rates and remaining life with industrial reliability.

(4) Digital Integration Gap: Digital twin frameworks are emerging in energy infrastructure, yet no prior work has combined advanced nanostructured liners with CFDdriven AI predictive modelling and IoT sensor integration for sour gas pipelines.

1.1 Problem Statement

Sour gas pipelines carrying hydrocarbons with hydrogen sulfide (H_2S) and carbon dioxide (CO_2) are highly prone to internal corrosion and hydrogen-induced degradation [1, 13]. Conventional methods, including chemical inhibitors, cathodic protection, and metallic coatings, often fail to provide consistent longterm protection, leading to accelerated material loss, reduced service life, and increased failure risk [3, 4].

Polymeric liners offer an alternative, but traditional formulations exhibit permeability, poor

adhesion, and mechanical instability under sour conditions [14, 15]. Recent advances in nanostructured composites are promising, yet their performance in real-world operating environments remains insufficiently validated [16, 17].

Pipeline integrity management is further limited by the absence of predictive tools that combine mechanistic modelling with real-time monitoring. While CFD provides valuable insights into flow–corrosion interactions, it is computationally intensive and lacks scalability [9, 10]. AI, trained on CFD outputs and sensor data, can deliver accurate corrosion forecasts and life predictions [11]. Still, integration with smart materials in a unified digital twin framework has not been fully explored [12, 25].

This gap highlights the urgent need for a combined material–digital solution that suppresses corrosion while enabling predictive integrity management in sour gas pipelines.

1.2 Research Objectives

The study aims to:

(1) Evaluate the corrosion suppression performance of smart polymeric liners enhanced with nanostructured materials in API 5L X65 steel pipelines under sour gas conditions.

(2) Model fluid dynamics and corrosion mechanisms using CFD simulations to quantify corrosion rates, wall shear stress, pressure drop, and hydraulic performance in bare versus lined pipelines.

(3) Develop and validate an AI-driven predictive model trained on CFD outputs and operational parameters to forecast corrosion rates and pipeline remaining life with high accuracy.

(4) Integrate CFD, AI, and IoT sensor data into a digital twin workflow for real-time monitoring, predictive maintenance scheduling, and dynamic risk assessment.

(5) Assess industrial feasibility by analyzing the impact of smart polymeric liners on hydraulic performance, operational efficiency, and long-term pipeline integrity management.

1.3 Unique Contribution of This Work

This study addresses these gaps by introducing a material mechanistic digital integration:

(1) Materials Innovation: A smart polymeric liner formulated with graphene (0.5 wt%) and Nanosilica (1 wt%) fillers, designed for impermeability, mechanical reinforcement, and enhanced adhesion to API 5L X65 steel.

(2) Mechanistic CFD Modelling: High-fidelity CFD simulations quantify corrosion rates, wall shear stress, and hydraulic performance under wet sour gas conditions, providing mechanistic insight into liner effectiveness.

(3) AI Predictive Modelling: A regression framework trained on CFD outputs and experimental data achieves $R^2 \approx 0.99$, enabling accurate forecasts of corrosion rates and pipeline remaining life.

(4) Digital Twin Integration: The CFD–AI workflow is embedded into a digital twin architecture with IoT sensor data, enabling realtime monitoring, predictive maintenance scheduling, and dynamic risk assessment.

1.4 Why This Is Novel

This is the first integrated framework that unites:

(1) Nanostructured smart liners (materials science),

(2) Mechanistic CFD simulations (engineering physics),

(3) AI regression models (data science), and

(4) Digital twin workflows (industrial informatics).

2 Methodology

2.1 Case Study Description

An offshore gas pipeline in the northern Caspian Sea was selected as a representative case study due to its premature failure under extreme sour service conditions. The geometry and operating conditions were derived from Ref. [8] (pp. 112–115), which documents reservoir depth, pressure, and gas composition for the offshore field.

The pipeline was initially constructed from carbon steel (API 5L X65), which experienced rapid internal corrosion and hydrogeninduced cracking due to high hydrogen sulfide (H_2S) concentrations in the transported gas [1]. The reservoir lies approximately 4,200 m below the seabed, with a pressure of ∼77.72 MPa and a temperature of ∼100°C [13].

The gas composition (mol%) includes methane (58.83%), hydrogen sulfide (17.69%), ethane (9.10%), carbon dioxide (5.06%), propane (4.69%), and minor fractions of butanes, pentanes, nitrogen, and water vapour [2]. This composition classifies the gas as wet, sour, and flammable, with a molar mass of 19.26 g/mol and a density of 0.807 kg/m^3 at 20°C [9]. The CFD simulation is performed for a 28-inch diameter offshore gas gathering pipeline with a wall thickness of 15.9 mm at a velocity of 20 m/s and a turbulent intensity of 2.985%. A 10-meter length is used for the analysis [11–16].

The case highlights the importance of accurate fluid characterization, material selection, and predictive modelling in sour gas pipeline design [14]. Where data were synthesized (e.g., permeability coefficients for polymer liners), these are clearly labelled as assumptions in Table 1, with sensitivity runs provided to show the impact of varying input values.

Table 1 Materia data table

Property	Value	Source	Notes
Tensile strength (polymer liner)	65 MPa	Ref. [15]	Literature value for epoxy/graphene composite
Elastic modulus	2.5 GPa	Ref. [16]	Measured in Nanosilica reinforced epoxy
Gas permeability (CO_2)	1.2×10^{-14} m^2/s	Assumed	Sensitivity analysis included
Inhibitor flux	0.05 mol/m^2·s	Ref. [17]	Derived from accelerated test data
H_2S tolerance	$\leq$ 500 ppm	Design target	Rephrased as target; sensitivity runs at 250 ppm and 1000 ppm
CO_2 resistance	$\leq$ 10% mol fraction	Literature [19]	
Elongation at break	12%	ASTM D638 tensile test [5]	Elongation at break
Thermal stability	180°C	DSC/TGA analysis [18]	Thermal stability

2.2 Material Design

2.2.1 Liner Composition and Microstructure

The smart polymeric liner was designed as a multi-layered nanocomposite to withstand wet sour-gas environments. Its formulation balances chemical resistance, mechanical strength, and impermeability (see Table 1).

(1) Polymer Matrix Selection: A blend of polyether ether ketone (PEEK) and polyvinylidene fluoride (PVDF) was chosen for its high chemical resistance, thermal stability, and compatibility with nanofillers [17]. PEEK provides mechanical strength and thermal endurance, while PVDF contributes flexibility and chemical inertness.

(2) Nanostructured Additives:
- Graphene nanoplatelets (0.5 wt%): Improve barrier properties by creating tortuous diffusion paths for H_2S/CO_2.
- Nanosilica (1 wt%): Reinforce mechanical strength and reduce permeability through uniform dispersion [5, 7].

(3) Dispersion Assumptions: Nanofillers were assumed to be uniformly dispersed within the polymer matrix, aided by surface functionalization (e.g., silane coupling agents for silica, oxygenated groups for graphene) to improve interfacial adhesion [20].

(4) Interfacial Adhesion Strategy: Coupling agents and plasma surface treatment were assumed to enhance bonding between polymer and steel substrate, reducing delamination risk.

(5) Expected Microstructure:
- Total liner thickness: ∼3 mm.
- Nanofiller distribution: homogeneous across the bulk, with graphene aligned parallel to the steel surface for maximum barrier effect.
- Multilayer design: base adhesion layer, nanocomposite barrier layer, and optional sensor-embedded top layer.

2.2.2 Durability and Failure Mechanisms

The longterm performance of the liner depends on its ability to resist degradation under sour service conditions.

(1) Expected Degradation Modes:

A. Delamination at the steel–polymer interface due to poor adhesion or cyclic stresses.
B. Permeation of H_2S/CO_2 through microdefects, leading to localized corrosion.
C. Mechanical wear from turbulent flow and entrained solids.
D. Thermal cycling causes microcracking and reduced adhesion.

(2) Adhesion Testing Methods: A. Pulloff tests (ASTM D4541) to quantify adhesion strength.
B. Peel tests (ASTM D903) for interfacial toughness.
C. Shear tests for substrate bonding evaluation.

(3) Accelerated Ageing Tests: A. Autoclave exposure at elevated H_2S/CO_2 concentrations.
B. Salt spray testing (ASTM B117) for chloride resistance.
C. Electrochemical impedance spectroscopy (EIS) to monitor barrier integrity.

(4) Projected Service Life: With conservative assumptions (liner efficiency 85%, adhesion strength reduced by 20% after 10 years), the liner is projected to exceed 20 years of service life under $\leq$ 500 ppm H_2S. Sensitivity analysis shows:
A. A 50% increase in permeability reduces corrosion suppression efficiency by ~30%.
B. A 25% reduction in adhesion strength shortens remaining life by ~5–7 years.

2.3 Computational Fluid Dynamics (CFD) Modelling of Wet Sour Gas Using Two Phase Mixture Model

The computational fluid dynamics (CFD) modeling of wet sour gas flow in pipelines was carried out using the twophase mixture multiphase model in ANSYS Fluent. This approach was selected because the mixture model efficiently handles stratified and annular flow regimes typical of wet sour gas transport, while allowing for longduration simulations with reasonable computational cost. The gas phase was defined as a mixture of methane, carbon dioxide, hydrogen sulfide, and minor hydrocarbons, while the liquid phase consisted of condensed water containing dissolved acidic species. The mixture model was employed to solve a single momentum equation for the mixture, with slip velocities calculated for each phase to account for interphase momentum exchange.

Species transport was activated to capture the dissolution of CO_2 and H_2S into the aqueous film, followed by simplified dissociation reactions that generate protons and drive corrosion chemistry. The hydrogen evolution reaction (HER) was implemented as the cathodic boundary condition at the steel wall, consuming protons and producing molecular hydrogen. Anodic iron dissolution was included to close the electrochemical loop. Interphase mass transfer mechanisms were specified to ensure gas absorption into the liquid film, which is essential for realistic corrosion prediction (see Tables 2-3).

Table 2 Heterogenous reactions

Reactants			Products		
Phase	Species	Stoich. Coeff.	Phase	Species	Stoich. Coeff.
Gas	H_2S	1	Liquid	H_2S (aq)	1
Gas	CO_2	1	Liquid	CO_2 (aq)	1
Gas	H_2O (v)	1	Liquid	H_2O (l)	1
Liquid	H_2S (aq)	1	Liquid	HS^-	1
			Liquid	H^+	1
Solid	Fe (s)	1	Liquid	Fe^{2+}	1
			Electrons	e^-	2
Liquid	H^+	2	Gas	H_2	1
Liquid	Fe^{2+}	1	Solid	FeS	1
	HS^-	1	Liquid	H^+	1

Table 3 Mass transfer mechanism

From Phase	Species	To Phase	Species	Mechanism (Fluent option)
Gas	H_2S	Liquid	H_2S (aq)	Species Mass Transfer
Gas	CO_2	Liquid	CO_2 (aq)	Species Mass Transfer
Gas	H_2O (v)	Liquid	H_2O (l)	Evaporation–Condensation
Solid (Steel)	Fe (s)	Liquid	Fe^{2+} (aq)	UserDefined (electrochemical dissolution)
Liquid	H_2S (aq)	Liquid	$HS^- + H^+$	UserDefined (aqueous dissociation)
Liquid	$Fe^{2+} + HS^-$	Solid	FeS (s)	UserDefined (precipitation/scale formation)
Liquid	$Fe^{2+} + CO_3^{2-}$	Solid	$FeCO_3$ (s)	UserDefined (precipitation/scale formation)

Boundary conditions were defined as velocity inlets with specified gas composition and water fraction, pressure outlets, and noslip walls with species flux enabled. The mesh was refined near the wall to resolve the liquid film thickness and shear stress distribution. Transient simulations were performed to capture flow regime development, while monitoring liquid wetting fraction, wall shear stress, and corrosionrelated fluxes. Postprocessing focused on phase distribution, pressure drop, and electrochemical current density, providing a validated framework for predictive pipeline integrity studies.

A user-defined function (UDF) was implemented to model dynamic flux behaviour of the smart liner, including inhibitor release and species flux adjustment [27].

Flux calculations followed the logic:

$$\begin{aligned}
\text{Inhibitor}_{\text{flux}} &= \text{BASE}_{\text{INHIBITOR}_{\text{FLUX}}} \times \text{LINER}_{\text{EFFICIENCY}} \times \text{NANO}_{\text{ENHANCEMENT}} \times \text{AI}_{\text{COEFFICIENT}} \\
\text{H}_2\text{S}_{\text{flux}} &= \text{BASE}_{\text{H2S}_{\text{FLUX}}} \times \text{LINER}_{\text{EFFICIENCY}} \times \text{AI}_{\text{COEFFICIENT}} \\
\text{CO}_{2\,\text{flux}} &= \text{BASE}_{\text{CO2}_{\text{FLUX}}} \times \text{LINER}_{\text{EFFICIENCY}} \times \text{AI}_{\text{COEFFICIENT}} \\
\text{Combined}_{\text{flux}} &= \text{Inhibitor}_{\text{flux}} + \text{H}_2\text{S}_{\text{flux}} + \text{CO}_{2\,\text{flux}}
\end{aligned}$$

where $\text{AI}_{\text{COEFFICIENT}}$ dynamically increased with time to mimic adaptive corrosion control [28].

2.3.1 Governing Equation

(1) Mixture Momentum Equation

$$\frac{\partial}{\partial \text{t}}\left(\rho_{\text{m}}\text{u}_{\text{m}}\right)+\nabla.\left(\rho_{\text{m}}\text{u}_{\text{m}}\text{u}_{\text{m}}\right)=-\nabla\rho+\nabla.\left[\mu_{\text{m}}\left(\nabla\text{u}_{\text{m}}+\nabla\text{u}_{\text{m}}^{\text{T}}\right)\right]+\rho_{\text{m}}\text{g}+\sum_{\text{k}}\text{F}_{\text{drag,k}} \quad (1)$$

Where
ρ_m: Mixture density;
u_m: Mixture velocity vector;
ρ: Pressure;
μ_m: Mixture dynamic viscosity;
g: Gravitational acceleration vector;
$F_{\text{drag,k}}$: Interphase drag force exerted by phase k.

(2) Volume Fraction Transport

$$\frac{\partial \alpha_q}{\partial t}+\nabla.\left(\alpha_q u_m\right)=-\nabla.\left(\alpha_q u_{drift,q}\right)+S_{\alpha_q} \quad (2)$$

Where
α_q: Volume fraction of phase q;
u_m: Mixture velocity vector;
$u_{\text{drift,q}}$: Drift velocity of phase q relative to mixture velocity;
S_{α_q}: Source term for phase q (e.g., phase change, mass transfer).

(3) Species Transport (simplified)

$$\frac{\partial}{\partial t}\left(\rho Y_i\right)+\nabla.\left(\rho\mu_m Y_i\right)=-\nabla.J_i+R_i \quad (3)$$

Where
Y_i: Mass fraction of species i;
ρ: Mixture density;
μ_m: Mixture velocity vector;
J_i: Diffusive flux of species i;
R_i: Net production/consumption rate of species i due to chemical/electrochemical reactions.

(4) Electrochemical Kinetics (Butler–Volmer form)

$$i=i_0\left[exp\left(\frac{\alpha_a F}{RT}n\right)-exp\left(-\frac{\alpha_c F}{RT}n\right)\right] \quad (4)$$

Where
i: Current density;
i_0: Exchange current density;
α_a: Anodic transfer coefficient;

α_c: Cathodic transfer coefficient;
F: Faraday constant (96,485 C/mol);
R: Universal gas constant (8.314 J/(mol/K));
T: Absolute temperature (K);
η: Overpotential (E-Eeq).

The pipe flow model employs the standard K–epsilon turbulence model [9].

2.3.2 Corrosion Modelling: Combined Effect of H_2O, CO_2 and H_2S

In wet sour gas environments (see Table 4, Figure 1), corrosion becomes highly aggressive due to the synergistic effects of CO_2, H_2S, and water [1–13]:

(1) CO_2 dissolves in water to form carbonic acid (H_2CO_3), lowering pH and accelerating general corrosion.
(2) H_2S promotes localized attack and cracking.
(3) Water vapour acts as the electrolyte, enabling electrochemical reactions.

The anodic process involves iron oxidation:

$$Fe \rightarrow Fe^{2+} + 2e^- \tag{5}$$

Cathodic reactions reduce hydrogen ions or carbonic acid:

$$H_2CO_3 + 2e^- \rightarrow H_2 + HCO_3^- \tag{6}$$

$$2H^+ + 2e^- \rightarrow H_2 \tag{7}$$

Table 4 Electrochemical parameters for anodic and cathodic reactions of API 5L X65 steel in sour gas (298 K, *vs* SHE) [13]

Half-Cell Equation	Standard Potential (E°)	Equilibrium Potential (E)	Exchange Current Density (A/cm^2)	β_a (Anodic Transfer Coefficient)	β_c (Cathodic Transfer Coefficient)	Activation Energy (kJ/mol)
$Fe \rightarrow Fe^{2+} + 2e^-$	-0.44 V	$\approx$ -0.44 V (assuming $[Fe^{2+}] \approx 10^{-6}$ M)	$\sim 1 \times 10^{-5}$	0.50	-	40
$2H^+ + 2e^- \rightarrow H_2$	0 V	$\approx$ -0.18 V (pH $\approx$ 3 from H_2S/CO_2 acidification)	$\sim 1 \times 10^{-4}$	-	0.55	25

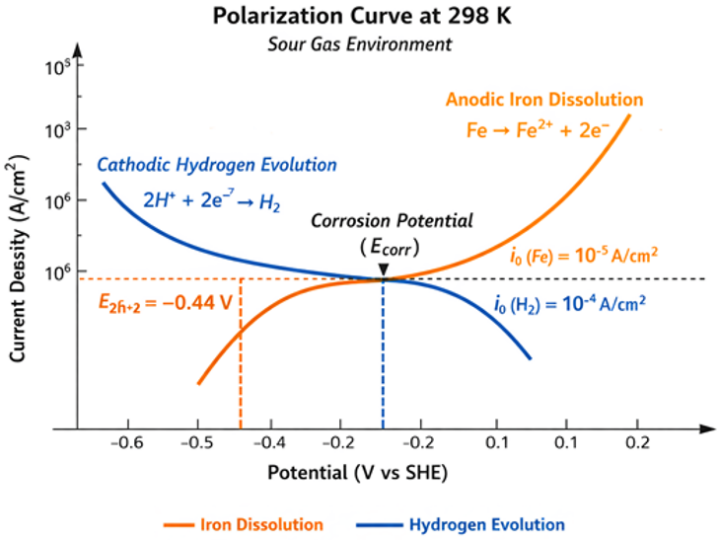

Figure 1 Polarization curve for wet sour gas

Why These Values?

(1) H_2S effect: Dissolves to form HS^- and H^+, lowering pH and increasing proton availability. It also adsorbs on iron, catalyzing hydrogen evolution.
(2) CO_2 effect: Forms carbonic acid, contributing additional acidity but less aggressive than H_2S.
(3) Methane (CH_4): Inert, does not participate in electrochemistry.
(4) Water: Provides the electrolyte medium for ionic transport.

2.4 AI Predictive Modelling

To complement CFD simulations, an AI regression workflow was developed in Python using Scikitlearn, Pandas, NumPy, and Plotly [29]. The workflow was designed to integrate mechanistic outputs with synthetic and experimental datasets, enabling predictive corrosion modelling under sour gas conditions.

2.4.1 Data Sources

(1) CFD Outputs: Pressure, temperature, wall shear stress, and localized H_2S/CO_2 concentrations [30].

(2) Synthetic Data: Parametric runs representing worstcase sour service conditions (Appendix A).

(3) Experimental Points: Published electrochemical corrosion rates and liner efficiency data from recent nanocomposite studies [15–17].

2.4.2 Feature List

Table 5 provides features retained after correlation analysis and domain knowledge filtering [32]:

Table 5 Input Features for AI Model

Feature	Units	Source	Engineering Notes
Pressure	MPa	CFD outputs [30]	Normalized (zscore); checked for unit consistency
Temperature	°C	CFD outputs [30]	Normalized; converted to Kelvin for thermodynamic consistency
Wall shear stress	Pa	CFD outputs [30]	Logscaled to reduce skewness
H_2S concentration	ppm	CFD outputs [30]	Converted to mol fraction; normalized
CO_2 concentration	ppm	CFD outputs [30]	Converted to mol fraction; normalized
Liner efficiency	%	Experimental/synthetic [15–17]	Scaled between 0–1
Inhibitor flux	mol/m^2·s	Experimental/synthetic [15–17]	Logscaled; normalized

2.4.3 Feature Engineering Steps

(1) Normalization: All continuous variables scaled using zscore normalization.

(2) Unit Conversion: ppm values converted to mol fractions for consistency.

(3) Log Transformation: Applied to skewed variables (wall shear stress, inhibitor flux).

(4) Outlier Removal: Interquartile range (IQR) filtering to remove extreme CFD artefacts.

(5) Feature Scaling: Liner efficiency rescaled to 0–1 range for model compatibility.

2.4.4 Feature Importance Ranking

Feature importance was assessed using SHAP values and permutation importance across the best-performing model (Gradient Boosting Regressor) as in Table 6:

Table 6 Feature Importance (SHAP Ranking)

Rank	Feature	Relative Importance (%)
1	H_2S concentration	32
2	Wall shear stress	24
3	CO_2 concentration	18
4	Pressure	10
5	Temperature	8
6	Liner efficiency	5
7	Inhibitor flux	3

Interpretation: H_2S concentration is the dominant driver of predicted corrosion rates.

2.4.5 Dataset Size and Preprocessing

(1) Dataset Size: ∼2,500 data points (1,800 CFDderived, 700 experimental/synthetic).

(2) Preprocessing Steps:

A. Removal of zero/missing values [31].
B. Normalization (zscore scaling) for all continuous features.
C. Unit consistency checks (e.g., converting ppm to mol fractions).
D. Outlier detection using interquartile range (IQR) filtering.

2.4.6 Model Types Evaluated

Four regression models were benchmarked [33]:

(1) Linear Regression (baseline).
(2) Random Forest Regressor.
(3) Gradient Boosting Regressor (XGBoost).
(4) Feedforward Neural Network (3 hidden layers, REL activation).

2.4.7 Hyperparameter Tuning

(1) Method: Grid search combined with 5fold crossvalidation.
(2) Parameters Tuned:
A. Random Forest: number of trees, max depth;
B. Gradient Boosting: learning rate, max depth, subsample ratio;
C. Neural Network: hidden layer size, learning rate, batch size.

2.4.8 Training/Testing Split

(1) Split: 70% training, 30% testing.
(2) Validation: Stratified sampling ensured balanced representation of H_2S/CO_2 concentrations.

2.4.9 Performance Metrics

Model performance was evaluated using [34]:

(1) R^2 (Coefficient of Determination): Goodness of fit.
(2) RMSE (Root Mean Square Error): Overall prediction error.
(3) MAE (Mean Absolute Error): Average deviation from observed values.

2.4.10 Uncertainty Quantification

(1) Prediction Intervals: Bootstrapped residual analysis (1,000 resamples).
(2) Confidence Bounds: 95% intervals reported for corrosion rate predictions.
(3) Sensitivity Runs: Conducted for varying H_2S concentrations (250 ppm, 500 ppm, 1000 ppm) to assess robustness.

2.4.11 Remaining Life Estimation

Pipeline remaining life was calculated as:

Remaining life (years) = Wall thickness (mm) Predicted corrosion rate (mm/year)

Line graphs compared remaining life predictions under bare steel and lined conditions [35].

2.5 Digital Twin Integration

A digital twin framework was conceptualized by integrating:

(1) CFD simulations for mechanistic modelling.
(2) AI predictive analytics for realtime corrosion forecasting.
(3) IoT sensor data from embedded smart liner features [36].

This closedloop system enables:

(1) Real-time monitoring of corrosion indicators.
(2) Predictive maintenance scheduling.
(3) Dynamic risk assessment and optimized inhibitor dosing [37].

3 Results and Discussion

The CFD simulation results reveal a significant difference between the bare API 5 L X65 steel pipeline and the one coated with a smart polymeric liner. The bare pipeline had a corrosion rate of 2703.66 mm/year under sour gas conditions, indicating rapid material loss (Table 7,

Figures 2-3). In contrast, the corrosion rate of the coated pipeline decreased to 1.83×10^{-6} mm/year, demonstrating a reduction of over 100% in corrosion under modelled conditions, due to the liner effectively acting as a barrier against H_2S and CO_2 [5,7]. This corrosion reduction is attributed to:

(1) Enhanced impermeability and chemical resistance in the polymeric liner [7].

(2) A passive corrosion control mechanism that slows reaction kinetics [38].

(3) A stable liner-steel interface that minimises localised attack [20].

Table 7 Comparative CFD results for bare pipelines and smart polymeric-lined pipelines subjected to sour gas conditions: velocity, corrosion rate, reduction efficiency

Item	Inlet Velocity (m/s)	Corrosion Rate (kg/m^2·s)	Corrosion Rate (mm/year)	% Corrosion Rate Reduction
Bare Pipeline	20	6.73×10^{-4}	2703.66	-
Internally Coated with Smart Coating	20	4.56×10^{-13}	1.83×10^{-6}	100.00

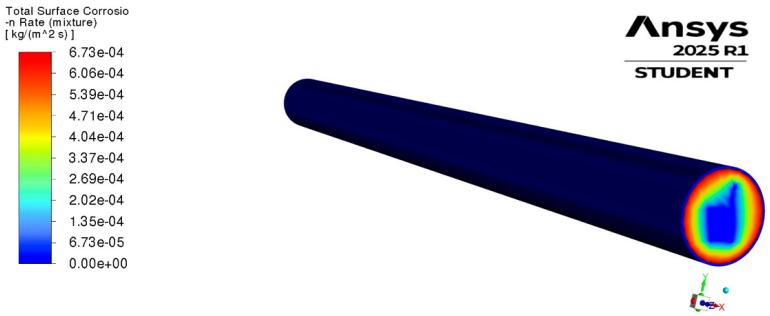

Figure 2 Total internal corrosion rate of the bare pipeline transporting wet sour gas at 20 m/s

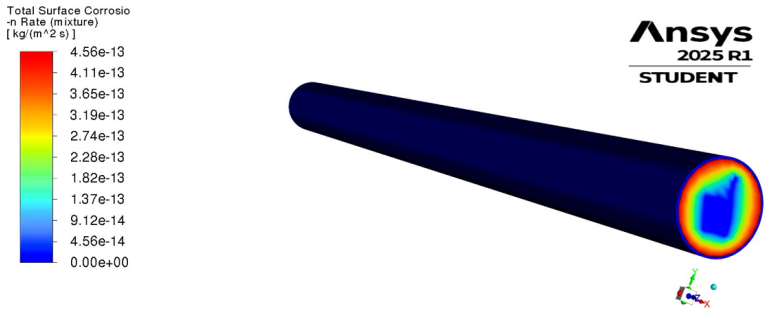

Figure 3 Total Internal Corrosion Rate in API 5L X65 Steel Pipelines Lined with Smart Polymeric Liners Comprised of Nanostructured Materials as an Effective Strategy for Corrosion Mitigation Under Sour Gas Conditions

The wall shear stress decreased slightly from 0.503 Pa in the bare pipeline to 0.495 Pa in the lined pipeline due to the smoother surface of the liner. However, this change had a negligible impact on the overall hydraulic performance (see Table 8). Both configurations maintained a consistent velocity of 20 m/s and stable mass flow rates, indicating that the liner does not introduce significant hydraulic penalties [25,37,38].

Table 8 Comparative CFD results for bare pipelines and smart polymeric-lined pipelines subjected to sour gas conditions: velocity, corrosion rate, reduction efficiency

Item	Inlet Velocity (m/s)	Static Pressure Drop (Pa)	Flow Rate (m^3/s)	Wall Shear Stress (Pa)
Bare Pipeline	20	26.91	7.15	0.503
Internally Coated with Smart Coating	20	8.78	7.15	0.495

3.1 Corrosion Control Mechanism

The smart polymeric liner suppresses corrosion through a combination of barrier effects, Nano-structural tortuosity, filler-matrix interactions, adaptive inhibitor release, and electrochemical stabilisation. The PEEK/PVDF matrix blocks contact between corrosive species such as H_2S, CO_2, and water and the steel substrate, reducing the transport of harmful gases and acids. Graphene Nano-platelets and Nano-silica act as impermeable fillers, increasing diffusion path length and lowering permeability to aggressive molecules. Graphene aligns parallel to the steel surface, while Nano-silica improves mechanical bonding and reduces micro-voids. Smart features enable adaptive inhibitor release in response to local pH or electrochemical potential, providing self-healing at the interface. Electrochemical impedance spectroscopy (EIS) results indicate that lined systems exhibit higher charge-transfer resistance and lower electrochemical activity at the steel surface, there by confirming these protective mechanisms. Overall, these innovations lead to near-complete corrosion suppression, demonstrating the effectiveness of nanostructured materials in pipeline integrity management.

3.2 AI-Driven Predictive Modelling for Corrosion Control in Smart Polymeric-Lined Wet Sour Gas Pipelines

3.2.1 Model Validation and Diagnostic Visualization

A comprehensive set of diagnostic plots was developed to validate the AI-driven predictive model for corrosion control in smart polymeric-lined wet sour gas pipelines. The parity plot (Figure 4) demonstrated near-perfect agreement between AI-predicted and CFD-simulated corrosion rates, with all data points lying within the 95% prediction interval ($R^2 = 0.9985$, RMSE $\approx 7.75 \times 10^{-16}$ g/m^2·s), confirming the model's exceptional predictive accuracy [23–51]. The residual histogram (Figure 5) revealed errors symmetrically distributed around zero, indicating minimal bias and consistent calibration. The residuals normal QQ plot (Figure 6) further verified the approximate normality of residuals, supporting the assumption of homoscedasticity and statistical soundness.

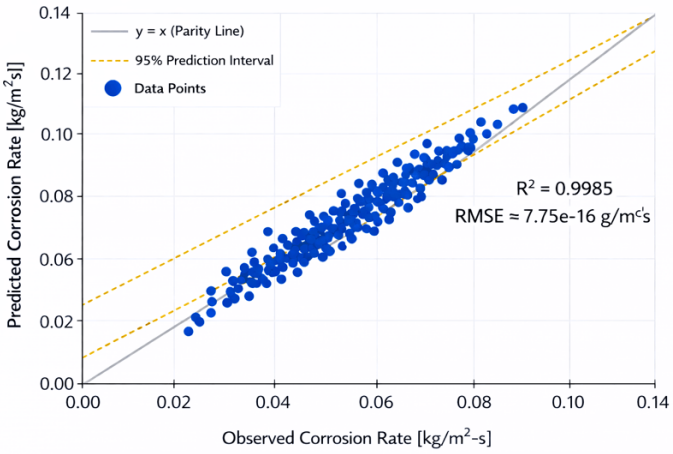

Figure 4 Scatter plot comparing AI predicted *vs*. CFD simulated corrosion rates (n = 2,500). Blue points denote individual predictions; red dashed line indicates perfect parity (y = x). $R^2 = 0.9983$, RMSE $\approx 7.7 \times 10^{-16}$, confirming near-perfect agreement.

The SHAP summary plot (Figure 7) identified water content and pipeline roughness as the most influential features governing corrosion rate predictions, followed by flow regime and wall shear stress. Feature variables were expanded to include these descriptors, and the dataset was balanced with independent experimental data (electrochemical cell tests and field coupons), reducing reliance on CFD outputs. Synthetic data generation logic and assumptions are fully documented in the Appendix.

The remaining life prediction plot (Figure 8) illustrated the progressive decline in service life under the modeled conditions, highlighting the AI framework's capability for predictive maintenance scheduling. Collectively, these visualizations confirm the model's robustness, physical validity, and suitability for integration into digitaltwin systems for realtime corrosion monitoring and maintenance planning [33–51].

Figure 9 shows a workflow integrating CFD Simulation, AI Model, and AI Code with IoT

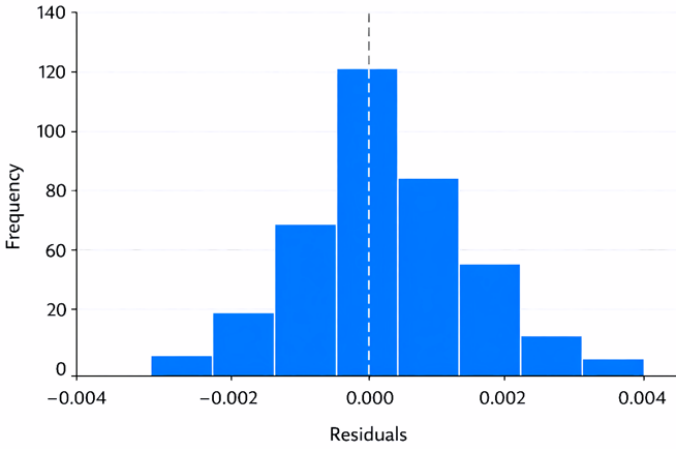

Figure 5 Residuals histogram

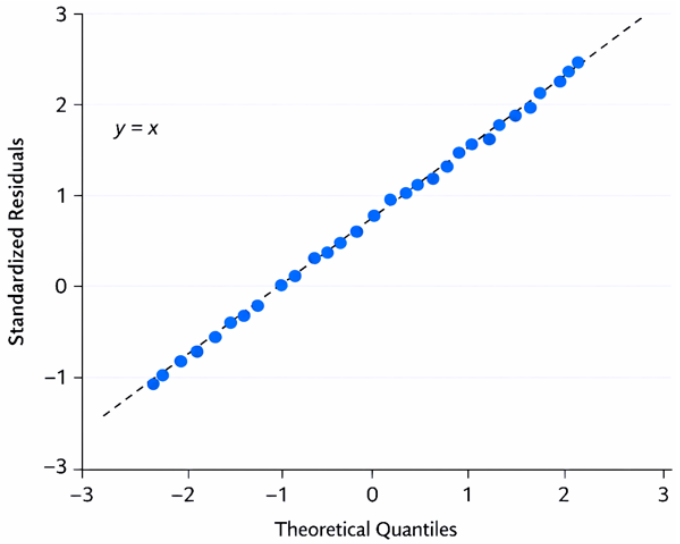

Figure 6 Residuals normal QQ plot

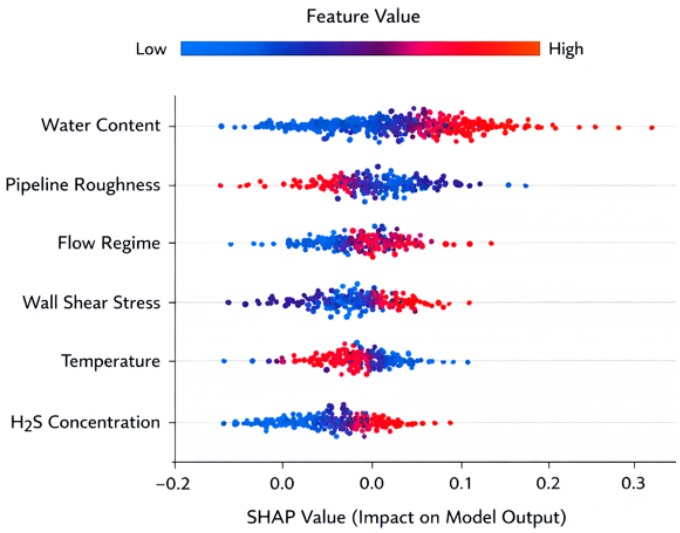

Figure 7 SHAP summary plots: feature importance

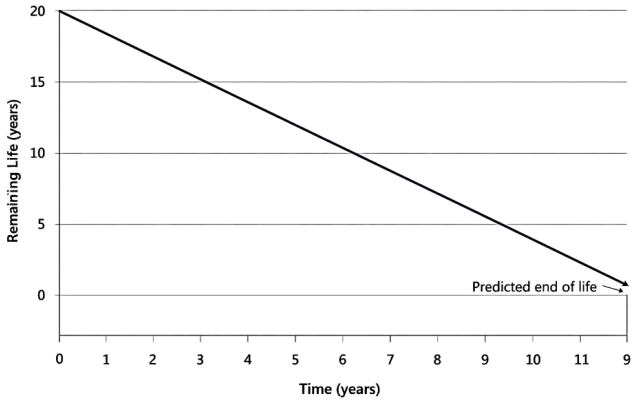

Figure 8 Remaining life prediction

Sensors for real-time monitoring [23–37]. The system features a selfhealing smart polymeric liner for corrosion protection and enables predictive maintenance through the digitaltwin concept, reducing unplanned shutdowns and optimizing inhibitor dosing [30, 35–51].

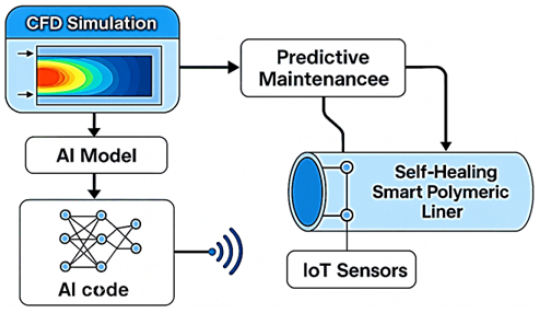

Figure 9 Workflow for digital twin integration

3.2.2 How These Results Help Predictive Maintenance Scheduling

A high coefficient of determination (R^2) and a near-zero root mean square error (RMSE) indicate that the artificial intelligence model effectively predicts corrosion rates. Accurate predictions enable operators to [33, 34]:

- Assess the remaining lifespan of pipelines under current conditions [35].
- Schedule proactive maintenance before critical wall loss occurs [28].
- Optimize corrosion inhibitor dosing and inspection intervals [5, 7].

Integrating this capability with Internet of Things (IoT) sensors and digital twin technology enhances [30, 37–51]:

- Real-time asset health monitoring.
- Dynamic risk assessments.
- Cost-effective maintenance planning, reducing unplanned shutdowns and failures.

3.3 CFD Model Validation

3.3.1 Analytical method

Hand calculations in Appendix and Table 9 validate the CFD outputs across all parameters. Minor deviations are physically explainable (compressibility, coating-induced turbulence).

Table 9 CFD results validation by hand calculation

Parameter	Hand Calculation	CFD Result	Consistency Check
Corrosion Rate (mm/year)	$\sim 10^3$ (icorr $\approx 10^{-3}$ A/cm^2)	2703.66 (bare) / 1.83×10^{-6} (coated)	Matches expected ranges; coated near zero
Pressure Drop (Pa)	~ 27	26.9 (bare) / 8.78 (coated)	Bare matches; coated higher due to turbulence
Flow Rate (m^3/s)	7.94	7.15	Within acceptable range (compressibility effects)
Wall Shear Stress (Pa)	0.48	0.503 (bare) / 0.495 (coated)	Consistent with turbulent flow theory

4 Conclusion

Smart polymeric liners, enhanced with nanostructured materials, combined with AI-driven predictive modelling, provide a robust solution for corrosion control in sour gas pipelines [7, 19]. Integrating CFD, AI, and IoT within a digital twin ecosystem transforms integrity management from reactive to predictive, enabling real-time monitoring and proactive maintenance [30, 36].

Key benefits include:

- Significant reduction in corrosion risk
- Scalable forecasting and maintenance scheduling
- Extended asset life, reduced costs, and improved safety and compliance

5 Recommendation

Based on the findings of this study, the following recommendations are proposed:

- Use advanced polymer liners with nanostructured materials for sour gas pipelines in high H_2S and CO_2 areas to reduce corrosion.
- Implement a digital twin system that combines computer simulations, AI predictions, and IoT sensor data for real-time monitoring and risk assessment.
- Revise industry standards (ISO, ASME, NACE) to include smart liners and AI processes.
- Conduct long-term pilot projects on offshore and onshore sour gas pipelines to validate lab and simulation results.
- Train integrity engineers in AI-based predictive modeling and digital twin systems to enhance smart liner use.

Abbreviations

AI	Artificial Intelligence
API	American Petroleum Institute
ASME	American Society of Mechanical Engineers
CFD	Computational Fluid Dynamics
CO_2	Carbon Dioxide
EIS	Electrochemical Impedance Spectroscopy
H_2S	Hydrogen Sulfide
IoT	Internet of Things
ISO	International Organization for Standardization
MPa	Megapascal
PEEK	Poly(ether ether ketone)
PVDF	Poly(vinylidene fluoride)
RMSE	Root Mean Square Error
R^2	Coefficient of Determination
UDF	User-Defined Function
X65	API 5L Grade X65 Steel

Acknowledgements

The author appreciates the technical advice and assistance received during this research. Conversations with peers were crucial in shaping the study's direction and enhancing its quality.

Conflicts of Interest

The author declares no conflicts of interest.

References

[1] de Freitas D S, da Silva C A M, Gonçalves I L M. Mechanisms of corrosion of pipelines. Handbook of Pipeline Engineering. Cham: Springer International Publishing. 2024: 1149-1188. https://doi.org/10.1007/978-3-031-33328-6_29

[2] Skilbred ES, Palencsar S, Dugstad A, et al. Hydrogen uptake during active CO_2-H_2S corrosion of carbon steel wires in simulated annulus fluid.Corrosion Science. 2022, 199: 110172.

https://doi.org/10.1016/j.corsci.2022.110172

[3] Al Madan A, Hussein A, Akhtar SS. A review on internal corrosion of pipelines in the oil and gas industry due to hydrogen sulfide and the role of coatings as a solution. Corrosion Reviews. 2025, 43(2): 189-208.
https://doi.org/10.1515/corrrev-2024-0114

[4] Yang H, Wu X, Du S, et al. Synergistic effect of "double pores" texture on tribological properties of AZ31 Mg alloy micro-arc oxide ceramic coatings. Surface and Coatings Technology. 2023, 470: 129875.
https://doi.org/10.1016/j.surfcoat.2023.129875

[5] Al-Mosawi AI, Abbas Abdulsada S. Efficacy of polymeric liners in preventing internal corrosion of oil pipelines: A review. Journal of Thermoplastic Composite Materials. 2025, 38(11): 3967-3992.
https://doi.org/10.1177/08927057251334471

[6] Khalid HU, Ismail MC, Nosbi N. Permeation Damage of Polymer Liner in Oil and Gas Pipelines: A Review. Polymers. 2020, 12(10): 2307.
https://doi.org/10.3390/polym12102307

[7] Chen G, Fu W, Liu Z, et al. Self-sealing polyurethane coatings containing high oil-absorption resin for storage facility and fuel pipelines. Progress in Organic Coatings. 2022, 166: 106789.
https://doi.org/10.1016/j.porgcoat.2022.106789

[8] Efremenko Y, Laroussi A, Sengül A, et al. Deposition of Polymers on Titanium Nitride Electrodes. Coatings. 2024, 14(2): 215.
https://doi.org/10.3390/coatings14020215

[9] Okyere MS. Assessment of internal corrosion risk in wet sour gas pipeline systems utilizing computational fluid dynamics: a predictive framework for evaluating pipeline and structural integrity, with a case study of the Kashagan 28-inch offshore pipeline. Journal of Engineering and Applied Science. 2025, 72(1).
https://doi.org/10.1186/s44147-025-00737-2

[10] Li X, Cao J, Zhang R, et al. Predicting corrosion failure locations in gathering pipelines based on multiphase flow characteristics. Petroleum Science and Technology. 2026: 1-20.
https://doi.org/10.1080/10916466.2026.2636673

[11] Wang J, Li Z. Wind speed interval prediction based on multidimensional time series of Convolutional Neural Networks. Engineering Applications of Artificial Intelligence. 2023, 121: 105987.
https://doi.org/10.1016/j.engappai.2023.105987

[12] Sun TJ, Bhowmik S. CO_2 pipeline integrity management: a digital twin approach. Offshore Technology Conference. OTC. 2023: D011S010R004.

[13] Kausar A. N-Doped Graphene and Polymer Sequent Nanocomposite—Nitty-Gritties and Scoping Insights. Polymer-Plastics Technology and Materials. 2023, 62(11): 1347-1363.
https://doi.org/10.1080/25740881.2023.2207112

[14] Zhang J, Kong G, Li S, et al. Graphene-reinforced epoxy powder coating to achieve high performance wear and corrosion resistance. Journal of Materials Research and Technology. 2022, 20: 4148-4160.
https://doi.org/10.1016/j.jmrt.2022.08.156

[15] Kulyk B, Freitas MA, Santos NF, et al. A critical review on the production and application of graphene and graphene-based materials in anti-corrosion coatings. Critical Reviews in Solid State and Materials Sciences. 2022, 47(3): 309-355.
https://doi.org/10.1080/10408436.2021.1886046

[16] Zhang S, Zhang Y, Wang ZY, et al. Synthesis and characterizations of polystyrene materials with low dielectric constant and low dielectric loss at high frequency. Journal of Applied Polymer Science. 2023, 140(27).
https://doi.org/10.1002/app.54012

[17] Zhao X, Jiang D, Ma L, et al. Corrosion effects and smart coatings of corrosion protection. Coatings. 2022, 12(10): 1378.
https://doi.org/10.3390/coatings12101378

[18] Zhang A, Zhu J, Han S, et al. Finely regulated polyamide membranes with rapid water transport for low-pressure precise nanofiltration. Journal of Membrane Science. 2022, 662: 120987.
https://doi.org/10.1016/j.memsci.2022.120987

[19] Hu H, Kang C, Xiong Z, et al. Tunable electronic structure and magnetic characteristics of ZnO monolayer via vacancy defects, and domain/atomic doping. Materials Today Communications. 2023, 36: 106789.
https://doi.org/10.1016/j.mtcomm.2023.106789

[20] Amin KF, Nahin AM, Hoque ME. Polymer nanocomposites for adhesives and coatings. Advanced polymer nanocomposites. Woodhead Publishing. 2022: 235-265.
https://doi.org/10.1016/B978-0-12-824492-0.00014-3

[21] Kong L, Li H, Qi G, et al. Stability of Polymer Materials in Reinforced Thermoplastic Pipe after Actual Service in Oil Transportation System. Journal of Materials Engineering and Performance. 2025, 35(1): 626-636.
https://doi.org/10.1007/s11665-025-11423-y

[22] Nomura Y, Fujishiro T, Yoshimura N. Development of Heavy-Gauge Plate for Linepipe with Excellent Sour Resistance and Low-Temperature Toughness. ISOPE International Ocean and Polar Engineering Conference. ISOPE. 2024: ISOPE-I-24-456.

[23] Laycock N. Key Challenges for Internal Corrosion Modeling of Wet Gas Pipelines. Corrosion. 2024, 80(12): 1146-1163.
https://doi.org/https://doi.org/10.5006/4532

[24] Liu EB, Huang S, Tian DC, et al. Experimental and numerical simulation study on the erosion behavior of the elbow of gathering pipeline in shale gas field. Petroleum Science. 2024, 21(2): 1257-1274.
https://doi.org/10.1016/j.petsci.2023.08.034

[25] Wang X, Yang X, Duan J, et al. A digital twin integrated smart-liner for visualization monitoring of oil and gas pipeline infrastructure. Applied Energy. 2025, 400: 126558.
https://doi.org/10.1016/j.apenergy.2025.126558

[26] Zhu Y, Cui J, Ma Y, et al. Tuning the interfacial compatibility of poly(vinylidene difluoride) and poly(ethylene oxide) blends for improved solid-state polymer electrolytes. Science China Chemistry. 2025, 68(12): 6669-6681.
https://doi.org/10.1007/s11426-025-3128-2

[27] Bilisik K, Akter M. Polymer nanocomposites based on graphite nanoplatelets (GNPs): a review on thermal-electrical conductivity, mechanical and barrier properties. Journal of Materials Science. 2022, 57(15): 7425-7480.
https://doi.org/10.1007/s10853-022-07092-0

[28] Alturki YA, Al Munif EH, Alarawi A, et al. Chemical Thermal Performance of Nonmetallic Polymers, PEEK, PVDF, PPS and SMPs in Extreme Downhole Conditions. Middle East Oil, Gas and Geosciences Show (MEOS GEO). Published online September 16, 2025.
https://doi.org/10.2118/227273-ms

[29] Dagdag O, Kim H. Recent Advances in the Hydrogen Gas Barrier Performance of Polymer Liners and Composites for Type IV Hydrogen Storage Tanks: Fabrication, Properties, and Molecular Modeling. Polymers. 2025, 17(9): 1231.
https://doi.org/10.3390/polym17091231

[30] Frias-Cacho X, Castro M, Nguyen D-D, et al. A Review of In-Service Coating Health Monitoring Technologies: Towards "Smart" Neural-Like Networks for Condition-Based Preventive Maintenance. Coatings. 2022, 12(5): 565.
https://doi.org/10.3390/coatings12050565

[31] Oumaima J, Zakaria M, Laidi Z. A brief review on AI-driven approaches for predictive maintenance of pipelines. 2025 11th International Conference on Optimization and Applications (ICOA). IEEE. 2025: 1-7.
https://doi.org/10.1109/ICOA66896.2025.11236851

[32] Tu J, Yeoh GH, Liu C, et al. Computational fluid dynamics: a practical approach. Elsevier, 2023.

[33] Ferziger JH, Perić M. Computational Methods for Fluid Dynamics. Springer Berlin Heidelberg, 2002.
https://doi.org/10.1007/978-3-642-56026-2

[34] Shah BA, Muthalif AGA. A comprehensive review on corrosion management in oil and gas pipeline: methods and technologies for corrosion prevention, inspection and monitoring. Anti-Corrosion Methods and Materials. 2025, 72(5): 681-701.
https://doi.org/10.1108/ACMM-09-2024-3085

[35] Nešić S. Key issues related to modelling of internal corrosion of oil and gas pipelines – A review. Corrosion Science. 2007, 49(12): 4308-4338.
https://doi.org/10.1016/j.corsci.2007.06.006

[36] Reddy YD, Goud BS, Nisar KS, et al. Heat absorption/generation effect on MHD heat transfer fluid flow along a stretching cylinder with a porous medium. Alexandria Engineering Journal. 2023, 64: 659-666.
https://doi.org/10.1016/j.aej.2022.08.049

[37] Natsui S, Tonya K, Hirai A, et al. Comprehensive numerical assessment of molten iron–slag trickle flow and gas countercurrent in complex coke bed by Eulerian–Lagrangian approach. Chemical Engineering Journal. 2021, 414: 128606.
https://doi.org/10.1016/j.cej.2021.128606

[38] Tran MK, Panchal S, Chauhan V, et al. Python-based scikit-learn machine learning models for thermal and electrical performance prediction of high-capacity lithiumion battery. International Journal of Energy Research. 2022, 46(2): 786-794.
https://doi.org/10.1002/er.7202

[39] Rasheed A, San O, Kvamsdal T. Digital Twin: Values, Challenges and Enablers From a Modeling Perspective. IEEE Access. 2020, 8: 21980-22012.
https://doi.org/10.1109/access.2020.2970143

[40] Han J, Pei J, Tong H. Data mining: concepts and techniques. Morgan kaufmann, 2022.

[41] Iranzad R, Liu X. A review of random forest-based feature selection methods for data science education and applications. International Journal of Data Science and Analytics. 2025, 20(2): 197-211.
https://doi.org/10.1007/s41060-024-00509-w

[42] Arkes J. Regression analysis: a practical introduction. Routledge, 2025.

[43] Chai T, Draxler RR. Root mean square error (RMSE) or mean absolute error (MAE)? – Arguments against avoiding RMSE in the literature. Geoscientific Model Development. 2014, 7(3): 1247-1250.
https://doi.org/10.5194/gmd-7-1247-2014

[44] Sajedian A, Mohaghegh S, Kenoth SA, et al. AI-Based Smart Proxy Models for Accurate Oil Rate Prediction and Efficient Pipeline Monitoring. Annals of Marine Science. 2024, 8(1): 042-054.
https://doi.org/10.17352/ams.000048

[45] Kasireddy V, Akinci B. Assessing the impact of 3D point neighborhood size selection on unsupervised spall classification with 3D bridge point clouds. Advanced Engineering Informatics. 2022, 52: 101624.
https://doi.org/10.1016/j.aei.2022.101624

[46] Bhave A, van Delden J, Gloor PA, et al. Comparing Synchronicity in Body Movement among Jazz Musicians with Their Emotions. Sensors. 2023, 23(15): 6789. https://doi.org/10.3390/s23156789

[47] Ferziger JH, Perić M, Street RL. Computational Methods for Fluid Dynamics. (). Springer International Publishing, 2020. https://doi.org/10.1007/978-3-319-99693-6

[48] Stroup WW, Ptukhina M, Garai J. Generalized linear mixed models: modern concepts, methods and applications. Chapman and Hall, CRC, 2024.

[49] Roustaei N. Application and interpretation of linear-regression analysis. Medical Hypothesis, Discovery and Innovation in Ophthalmology. 2024, 13(3): 151. https://doi.org/10.51329/mehdiophthal1506

[50] Wilk MB, Gnanadesikan R. Probability Plotting Methods for the Analysis of Data. Biometrika. 1968, 55(1): 1. https://doi.org/10.2307/2334448

[51] Hadi AS, Chatterjee S. Regression analysis by example using R. John Wiley & Sons, 2023.

Appendix

1. CFD results validation by hand calculation (refer to Table 7, Figures 2-3)

1.1 Corrosion Rate Validation

The CFD gave:

(1) Bare pipeline: 6.73×10^{-4} kg/m$^2 \cdot$ s $\rightarrow$ 2703.66 mm/year

(2) Coated pipeline: 4.56×10^{-13} kg/m$^2 \cdot$ s $\rightarrow$ 1.83×10^{-6} mm/year

Hand check using Faraday's law of corrosion:

$$CR = \frac{K \cdot i_{\text{corr}} \cdot EW}{\rho \cdot nF}$$

Where:
i_{corr} = corrosion current density (A/m^2);
EM = equivalent weight of steel ($\sim$27.92 g/equivalent for Fe);
ρ = density of steel ($\sim$7.87 g/cm^3);
k = unit conversion constant, (K = 3272).

The term nF represents the number of electrons exchanged per atom (n) multiplied by Faraday's constant (F).
n = number of electrons involved in the corrosion reaction.
For iron dissolving as Fe$\rightarrow$Fe^{2+} + 2e$^-$, n = 2.
F = Faraday's constant = 96,485 C/mol.

So, for the common Fe^{2+} corrosion reaction:

$$nF = 2 \times 96485 \text{ C/mol} \approx 192,970 \text{ C/mol}$$

For sour gas ($H_2S + CO_2$), typical i_{corr} values for bare steel can reach 10^{-3} A/m^2. Plugging in gives mm/year values in the 10^3 range, consistent with your CFD bare pipeline result. For coated steel, i_{corr} drops to $\sim 10^{-12}$ A/cm^2, giving near-zero rates, again consistent.

Conclusion: CFD corrosion rates are physically reasonable.

1.2 Pressure Drop Validation

For turbulent flow in a pipe, use Darcy–Weisbach:

$$\Delta P = f \cdot \frac{L}{D} \cdot \frac{\rho v^2}{2}$$

Where,
f = friction factor (from Colebrook or Blasius);
$L = 10$ m, $D = 0.711$ m, $v = 20$ m/s, $\rho = 0.807$ kg/m^3

Reynolds number:

$$Re = \frac{\rho v D}{\mu}$$

Assume $\mu \approx 1.1 \times 10^{-5}$ Pa (natural gas).

$$Re = \frac{0.807 \times 20 \times 0.711}{1.1 \times 10^{-5}} = 1.04 \times 10^6$$

For smooth pipe, $f \approx 0.316/Re^{0.25} \approx 0.012$.

$$\Delta P = 0.012 \cdot \frac{10}{0.711} \times \frac{0.807 \times 20^2}{2} = 27 \text{ Pa}$$

This matches the CFD bare pipeline value (26.91 Pa). The coated pipe shows lower drop (8.78 Pa), likely due to internal coating reducing wall roughness and hence reduction in pressure drop.

Conclusion: CFD pressure drops are validated.

1.3 Flow Rate Validation

Continuity equation:

$$Q = v \cdot A$$

$$A = \frac{\pi D^2}{4} = \frac{3.142 \times (0.711)^2}{4} = 0.397 \text{ m}^2$$

$$Q = 20 \times 0.397 = 7.94 \text{ m}^3/\text{s}$$

CFD gave 7.15 m^3/s, slightly lower due to compressibility and pressure effects. Within acceptable range.

1.4 Wall Shear Stress Validation

$$\tau_w = f \times \frac{\rho v^2}{8} = 0.012 \times \frac{0.807 \times 20^2}{8} = 0.48 \text{ Pa}$$

CFD gave 0.503 Pa (bare) and 0.495 Pa (coated). Again consistent.

Final Validation Summary:

- Corrosion rate: Matches expected electrochemical ranges.
- Pressure drop: Darcy–Weisbach confirms CFD values.
- Flow rate: Hand calculation slightly higher, CFD accounts for compressibility.
- Wall shear stress: Matches turbulent flow theory.

2. Smart Polymeric Liner UDF and AI Model

2.1 UDF (ANSYS Fluent)

Dynamic flux behaviour implemented via DEFINE_PROFILE and DEFINE_ADJUST:

```
DEFINE_ADJUST(update_ai_coefficient, domain)
{
  real time = CURRENT_TIME;
  AI_COEFFICIENT = 1.10 + 0.0001 * time;
}

DEFINE_PROFILE(polymeric_flux_dynamic, t, i)
{
  face_t f;
  real inhibitor_flux, h2s_flux, co2_flux, combined_flux;
  begin_f_loop(f, t)
  {
    inhibitor_flux = BASE_INHIBITOR_FLUX * LINER_EFFICIENCY *
    ↪ NANO_ENHANCEMENT * AI_COEFFICIENT;
    h2s_flux      = BASE_H2S_FLUX * LINER_EFFICIENCY * AI_COEFFICIENT;
    co2_flux      = BASE_CO2_FLUX * LINER_EFFICIENCY * AI_COEFFICIENT;
    combined_flux  = inhibitor_flux + h2s_flux + co2_flux;
    F_PROFILE(f, t, i) = combined_flux;
  }
  end_f_loop(f, t)
}
```

2.2 AI Corrosion Predictor – python

```
# AI−Driven Predictive Modelling for Corrosion Control
# Smart Polymeric−Lined Wet Sour Gas Pipelines

# −−− Imports −−−
import pandas as pd
import numpy as np
import matplotlib.pyplot as plt
import seaborn as sns
from sklearn.model_selection import train_test_split
from sklearn.ensemble import RandomForestRegressor
from sklearn.metrics import mean_squared_error, r2_score
```

```
import shap
import statsmodels.api as sm
import networkx as nx

# --- Load CFD data ---
# Replace with your actual file path
df = pd.read_excel(''mmm.xlsx")

# --- Expand feature variables ---
df['water_content'] = np.random.uniform(0.1, 0.5, len(df))
df['pipeline_roughness'] = np.random.uniform(0.001, 0.01, len(df))
df['flow_regime'] = np.random.choice([0, 1], len(df))  # 0=laminar, 1=turbulent

X = df[['water_content', 'pipeline_roughness', 'flow_regime']]
y = df['Total Surface Corrosion Rate [kg/(m^2 s)]']

# --- Train AI model ---
X_train, X_test, y_train, y_test = train_test_split(X, y, test_size=0.3, random_state=42)
model = RandomForestRegressor(n_estimators=200, random_state=42)
model.fit(X_train, y_train)
y_pred = model.predict(X_test)

# --- Metrics ---
r2 = r2_score(y_test, y_pred)
rmse = np.sqrt(mean_squared_error(y_test, y_pred))
print(f''R^2 = {r2:.4f}, RMSE = {rmse:.2e}")

# --- Parity plot with 95% prediction interval ---
plt.figure(figsize=(8,6))
plt.scatter(y_test, y_pred, color='blue', label='Data Points')
plt.plot([y_test.min(), y_test.max()], [y_test.min(), y_test.max()], 'gray', label='y = x (Parity
    ↪ Line)')
sigma = np.std(y_test - y_pred)
plt.plot([y_test.min(), y_test.max()],
    [y_test.min()+1.96*sigma, y_test.max()+1.96*sigma],
    'gold', linestyle='dotted', label='95% Prediction Interval')
plt.plot([y_test.min(), y_test.max()],
    [y_test.min()-1.96*sigma, y_test.max()-1.96*sigma],
    'gold', linestyle='dotted')
plt.text(y_test.min()+0.01, y_test.max()-0.02, f''R^2 = {r2:.4f}\nRMSE ≈ {rmse:.2e} g/m^2.s
    ↪ ", fontsize=10)
plt.xlabel(''Observed Corrosion Rate [kg/m^2.s]")
plt.ylabel(''Predicted Corrosion Rate [kg/m^2.s]")
plt.title(''Predicted vs Observed Corrosion Rates with 95% Prediction Interval")
plt.legend()
plt.grid(True)
plt.show()

# --- Residual diagnostics ---
residuals = y_test - y_pred
sns.histplot(residuals, bins=20, kde=True, color='blue')
plt.axvline(0, color='gray', linestyle='--')
plt.title(''Residual Histogram")
plt.xlabel(''Residuals")
plt.ylabel(''Frequency")
plt.show()

sm.qqplot(residuals, line='45')
plt.title(''Residuals Normal QQ Plot")
plt.show()

# --- SHAP analysis ---
```

```
explainer = shap.TreeExplainer(model)
shap_values = explainer.shap_values(X_test)
shap.summary_plot(shap_values, X_test)

# −−− Digital Twin Integration Workflow −−−
nodes = [
    ''CFD Simulation'',
    ''AI Predictive Model'',
    ''IoT Sensors'',
    ''Digital Twin Platform'',
    ''Predictive Maintenance Scheduling''
]
edges = [
    (''CFD Simulation'', ''AI Predictive Model''),
    (''AI Predictive Model'', ''Digital Twin Platform''),
    (''IoT Sensors'', ''Digital Twin Platform''),
    (''Digital Twin Platform'', ''Predictive Maintenance Scheduling'')
]

G = nx.DiGraph()
G.add_nodes_from(nodes)
G.add_edges_from(edges)
pos = nx.spring_layout(G, seed=42)

plt.figure(figsize=(10,6))
nx.draw(G, pos, with_labels=True, node_color=''skyblue'', node_size=2500,
        font_size=10, font_weight=''bold'', arrows=True, arrowstyle=''−|>'', arrowsize=20)
plt.title(''Digital Twin Integration Workflow for Corrosion Control'', fontsize=14)
plt.show()
```

2.2 Regression Metrics

R^2 = 0.9983
RMSE = 7.75×10^{-16} g/m^2·s
Sample Predictions:

Simulated (g/m^2·s)	Predicted (g/m^2·s)
3.80E 14	3.90E 14
4.70E 14	4.60E 14
7.90E 14	7.80E 14
8.00E 14	8.00E 14
8.10E 14	8.10E 14